Decoding the CO_2 Reduction Mechanism of a Highly Active Organometallic Manganese Electrocatalyst: Direct Observation of a Hydride Intermediate and Its Implications

Sergio Fernández, Federico Franco,* Marta Martínez Belmonte, Sofia Friães, Beatriz Royo, Josep M. Luis,* and Julio Lloret-Fillol*

ABSTRACT: A detailed mechanistic study of the electrochemical CO_2 reduction catalyzed by the *fac*-[$Mn^I(CO)_3$(bis-^{Me}NHC)MeCN]$^+$ complex (**1-MeCN$^+$**) is reported herein by combining in situ FTIR spectroelectrochemistry (SEC), synthesis and characterization of catalytic intermediates, and DFT calculations. Under low proton concentrations, **1-MeCN$^+$** efficiently catalyzes CO_2 electroreduction with long catalyst durability and selectivity toward CO (*ca.* 100%). The [$Mn^{-I}(CO)_3$(bis-^{Me}NHC)]$^-$ anion (**1$^-$**) and the tetracarbonyl [$Mn^I(CO)_4$(bis-^{Me}NHC)]$^+$ complex (**1-CO$^+$**) are key intermediates of the catalytic CO_2-to-CO mechanism due to their impact on the selectivity and the reaction rate, respectively. Increasing the proton concentration increases formate production (up to 15% FE), although CO remains the major product. The origin of formate is ascribed to the competitive protonation of **1$^-$** to form a Mn(I) hydride (**1-H**), detected by SEC in the absence of CO_2. **1-H** was also synthesized and thoroughly characterized, including by X-ray diffraction analysis. Stoichiometric reactivity studies of **1-H** with CO_2 and labeled $^{13}CO_2$ indicate a fast formation of the corresponding neutral Mn(I) formate species (**1-OCOH**) at room temperature. DFT modeling confirms the intrinsic capability of **1-H** to undergo hydride transfer to CO_2 due to the strong σ-donor properties of the bis-^{Me}NHC moiety. However, the large potential required for the $HCOO^-$ release from **1-OCOH** limits the overall catalytic CO_2-to-$HCOO^-$ cycle. Moreover, the experimentally observed preferential selectivity for CO over formate is dictated by the shallow kinetic barrier for CO_2 binding to **1$^-$** compared to the Mn−H bond formation. The detailed mechanistic study highlights the reduction potential, pK_a, and hydricity of the metal hydride intermediate as crucial factors affecting the CO_2RR selectivity in molecular systems.

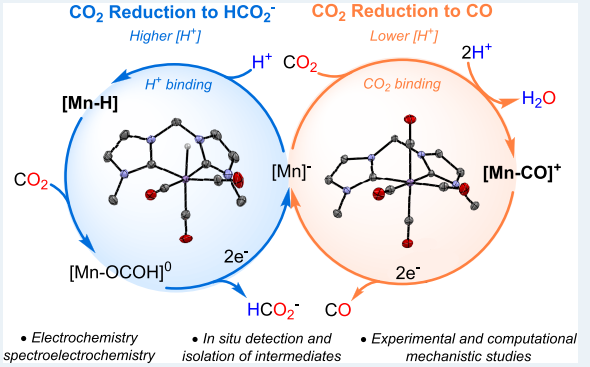

KEYWORDS: *electrocatalysis, CO_2 reduction, manganese, metal hydride, spectroelectrochemistry*

INTRODUCTION

The electrochemical CO_2 reduction reaction (CO_2RR) powered by renewable sources and promoted by transition metal-based catalysts is an attractive strategy to provide fuels or commodity chemicals.[1] However, due to the wide variety of potential carbon-based products of CO_2RR, a fundamental understanding of its catalytic mechanisms is crucial to systematically improve the performances by rational catalyst design and overcome the selectivity challenge for an efficient CO_2RR.[2]

Molecular electrocatalysts are characterized by having well-defined active sites, then serving as ideal platforms to investigate the reaction pathways by isolating the main intermediates involved in the process and by their study by *in situ* spectroelectrochemical (SEC) techniques.[3] Several organometallic complexes based on earth-abundant transition metals have been found to selectively convert CO_2 into carbon monoxide (CO), acting as homogeneous electrocatalysts in organic media.[4] Molecular catalysts have also shown promising performances when implemented in aqueous electrolyzers as heterogenized systems on carbon supports.[5] For some catalysts, the predominant formation of formate ($HCOO^-$) has been reported depending on the ligand structure or the reaction conditions, albeit a selective CO_2 conversion to $HCOO^-$ is achieved only in a few cases.[6] Since the seminal work by Deronzier and co-workers,[7] tricarbonyl Mn complexes with polypyridyl ligands, *e.g.*, [$Mn^I(CO)_3$(bpy)X] (bpy = 2,2′-

bipyridine), have been extensively studied as homogeneous molecular electrocatalysts for selective CO_2 reduction to CO.[8] The CO_2-to-CO conversion is primarily catalyzed by the electrogenerated two-electron ($2e^-$) reduced five-coordinate Mn anion species *via* competitive protonation-first or reduction-first pathways, depending on both the ligand structure and the reaction conditions (*e.g.*, the applied potential and the strength of the added proton source, see Scheme 1).[9] Minor amounts of

Scheme 1. General Mechanistic Proposal for *fac*-[Mn(CO)$_3$(bpy)Br] and Related Catalysts

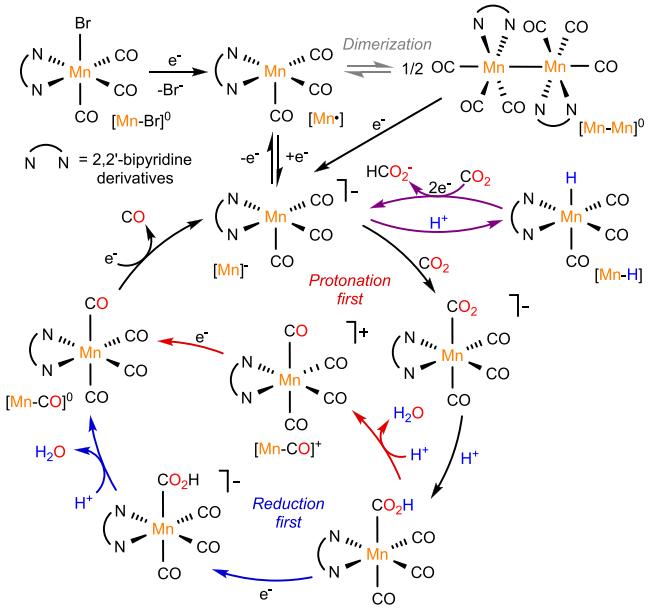

$HCOO^-$ were produced by a few examples of Mn catalysts with proton-responsive diimine ligands[10] as well as by some bpy-based Mn derivatives heterogenized on carbon electrodes in aqueous electrodes.[11] However, a predominant $HCOO^-$ formation was usually observed under pure photochemical conditions.[9c,12] Such a change of selectivity from CO to $HCOO^-$ was attributed to the competitive protonation of the anionic Mn catalyst to form a reactive Mn(I) hydride, which rapidly reacts with CO_2 (see Scheme 1). However, there is still a need to directly clarify the involvement and the role of Mn(I) hydrides in the $HCOO^-$ pathway.

Recently, the presence of tertiary amines as either pendant groups[6f] or additives[13] as well as concerted proton-electron transfer (CPET) mediators[14] has shown improved electrocatalytic formate production efficiencies. Under these conditions, suitable Brønsted acids, bpy-based Mn catalysts produced formate in high faradaic efficiencies (FEs). The presence of tertiary amine groups was proposed to mediate the formation of key Mn hydride intermediates. However, information about the Mn hydride species is limited and mainly derived from the *in situ* SEC data.[6f,10a,11a,15] Recently, Saouma and co-workers reported a thermochemical analysis of some *in situ* generated polypyridyl Mn(I) hydride complexes and experimental evidence of the CO_2 reaction with the Mn–H. Whereas the extreme instability of the parent complex with the unsubstituted bpy ligand prevented the observation of direct reactivity between Mn–H and CO_2, a Mn–formate species was obtained by reaction of Mn–H with CO_2 in the presence of bulky bpy ligands, which contribute to sterically protect the Mn–H and enhance its stability.[16] Still, the fundamental understanding of the CO_2 electroreduction mechanism leading to formate catalyzed by Mn electrocatalysts remains under investigation.

In recent years, *N*-heterocyclic carbene (NHC) ligands have been used as alternative platforms to polypyridyl diimine ligands in Mn complexes able to efficiently catalyze CO_2RR to CO with excellent selectivity in organic media.[17] In particular, we recently reported a tricarbonyl Mn-based catalyst bearing the bidentate methylene bis(*N*-methylimidazolium) (bis-^{Me}NHC) ligand, [Mn(CO)$_3$(bis-^{Me}NHC)Br] (**1-Br**) (Figure 1), which showed

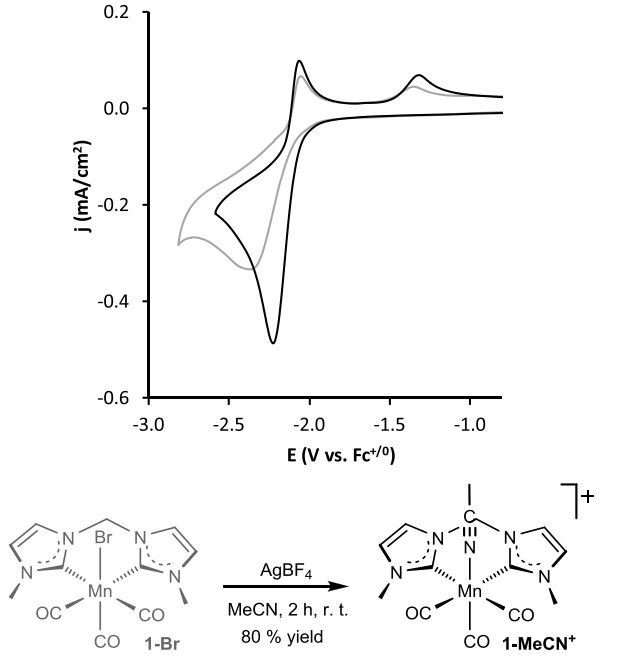

Figure 1. (Bottom) Synthesis of **1-MeCN**$^+$. (Top) CVs of **1-MeCN**$^+$ (1 mM, black) and **1-Br** (1 mM, gray) in an anhydrous electrolyte (0.1 M $TBAPF_6$/MeCN) under an Ar atmosphere.

extraordinary kinetics for selective CO_2-to-CO electroreduction in anhydrous acetonitrile (MeCN) or even in the presence of added water.[17a] Interestingly, increasing water concentrations led to a volcano-type dependence on the catalytic rate, with a maximum at *ca.* 1% v/v H_2O. We hypothesized that such an unexpected behavior could be due to a stable electrogenerated intermediate such as a Mn hydride species. To rationalize the origin of the peculiar electrocatalytic behavior with Brønsted acids, we aimed to investigate the key intermediates involved in the catalytic cycle and discuss their implications in the CO_2RR.

In this work, we report a thorough synergistic experimental and computational mechanistic investigation of the [Mn(CO)$_3$(bis-^{Me}NHC)(MeCN)]$^+$ (**1-MeCN**$^+$) electrocatalyst for CO_2RR in both aprotic and protic conditions. While the main catalytic pathway results in a highly efficient and selective CO_2-to-CO conversion in low-proton media, we shed light on the activation of a competitive mechanism leading to the catalytic production of $HCOO^-$ production in the presence of weak Brønsted acids. Furthermore, combining synthetic efforts with electrochemical and *in situ* FTIR-SEC techniques, we unambiguously characterized the key intermediates involved in the electrocatalytic pathways to CO and $HCOO^-$, respectively, establishing a direct correlation between their formation and the observed selectivity. This work provides new

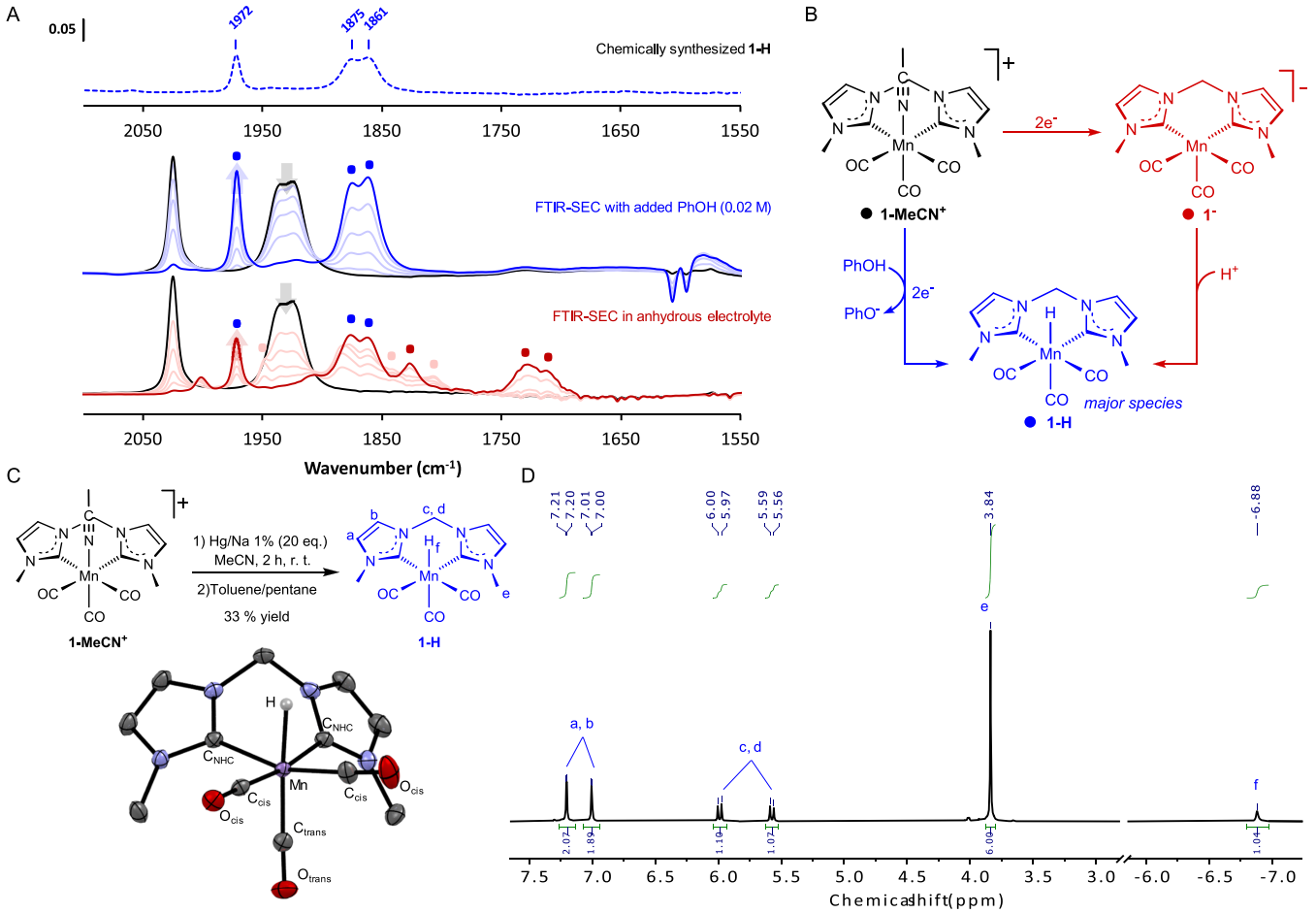

Figure 2. (A) FTIR-SEC of **1-MeCN**$^+$ (4 mM, black trace) in an anhydrous electrolyte (0.1 M $TBAPF_6$/MeCN), without (bottom) and with (middle) PhOH (0.02 M). Spectral changes upon reduction from black to dark red and blue lines, respectively. FTIR spectrum of the chemically synthesized **1-H** complex in CD_3CN (dashed blue trace). (B) Schematic representation of the reactivity observed by SEC under Ar without (red) and with (blue) PhOH. (C) Synthetic scheme of **1-H** and ORTEP structure (50% ellipsoid probability) obtained by XRD. Relevant bond distances (in Å): d(Mn−C_{cis}) = 1.807(2)−1.793(2); d(Mn−C_{trans}) = 1.807(2); d(Mn−C_{NHC}) = 2.0217(19)−2.017(2); d(C_{cis}−O_{cis}) = 1.154(3)−1.150(3); d(C_{trans}−O_{trans}) = 1.153(3). (D) ^{1}H NMR (400 MHz, CD_3CN) of **1-H**.

mechanistic insights, through well-defined and characterized intermediates, toward a fundamental understanding of the origin of selectivity in CO_2RR at the molecular level.

RESULTS AND DISCUSSION

Electrochemistry and Reactivity of 1-MeCN$^+$ under Ar.

The cationic **1-MeCN**$^+$ complex was prepared by the metathesis reaction with the $AgBF_4$ salt in MeCN from the corresponding Br-derivative, **1-Br** (Figure 1, see the SI). Compared to **1-Br**, **1-MeCN**$^+$ has better solubility in polar solvents, and the labile MeCN ligand is more convenient for synthetic and catalytic purposes. Furthermore, **1-MeCN**$^+$ also facilitates the characterization by *in situ* FTIR-SEC due to the lack of solvolysis equilibrium (see below).

Under Ar, the cyclic voltammograms (CV) in an anhydrous electrolyte (0.1 M $TBAPF_6$/MeCN) of **1-MeCN**$^+$ and **1-Br** display similar features. **1-MeCN**$^+$ presents a single 2e$^-$ reduction wave at −2.24 V (all the potentials reported are referenced *vs* $Fc^{+/0}$ redox couple), which is slightly more positive than the reduction peak observed for **1-Br** (Figure 1). A linear relationship of the peak current *vs* the square root of the scan rate indicates that the process is diffusion-limited (Figure S13).

The redox process of **1-MeCN**$^+$ in dry MeCN was monitored by *in situ* FTIR-SEC to investigate the main intermediate species involved (Figure 2A, bottom). At the open-circuit voltage, the spectrum of **1-MeCN**$^+$ shows three CO stretching frequencies typical of a tricarbonyl complex in a *fac* fashion (2025, 1935, and 1925 cm^{-1}, black trace). Upon negative applied bias (< −2.1 V), **1-MeCN**$^+$ converts into a mixture of two major species. The set of signals at lower energies (υ_{CO} at 1827, 1731, and 1713 cm^{-1}) corresponds to the doubly reduced five-coordinate [Mn(CO)$_3$(bis-^{Me}NHC)]$^-$ (**1**$^-$) anion (red dots), previously proposed as the species that binds CO_2 in the catalytic mechanism leading to CO production (Figure 2B).[17a] A transient species showing three signals at 1947, 1839, and 1805 cm^{-1} is also observed (pale pink dots), matching the DFT-calculated IR spectra of the neutral radical intermediate [Mn•] and the corresponding dimeric species [Mn−Mn] (Table S4). Although it was not univocally assigned to any specific species, a similar pattern was previously reported for an analogous Mn−NHC complex.[17d] In addition, the three intense bands at 1972, 1876, and 1862 cm^{-1} indicate the concomitant formation of a new species with a *fac*-Mn(CO)$_3$ coordination (blue dots). The same pattern was also detected during FTIR-SEC of **1-Br**, but a partial overlap with the spectral features of **1-Br** prevented its clear observation. Based on the comparison with the DFT-calculated IR data (*vide infra*) and with previous FTIR spectra assigned to polypyridyl Mn hydride species, we hypothesized

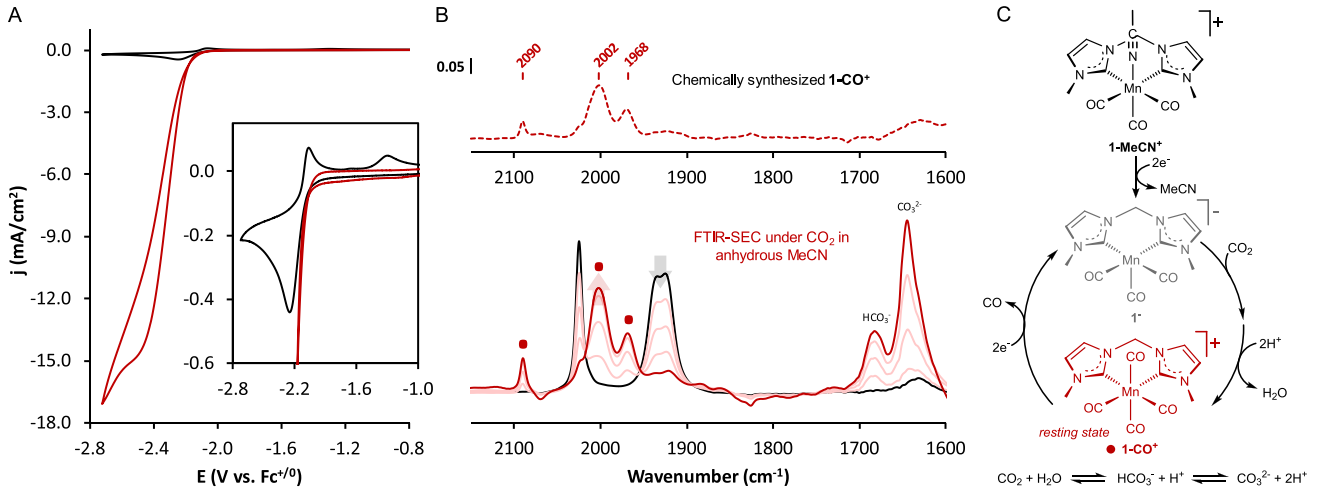

Figure 3. (A) CVs of **1-MeCN**$^+$ (1 mM) under Ar (black) and CO_2 atmospheres (red) in an anhydrous electrolyte (0.2 M $TBAPF_6$/MeCN). Scan rate = 100 mV s^{-1}. (B) Top, FTIR spectrum of the chemically synthesized **1-CO**$^+$ complex in MeCN (dashed red trace). Bottom, FTIR-SEC of **1-MeCN**$^+$ (4 mM, anhydrous 0.2 M $TBAPF_6$/MeCN) under CO_2, starting spectrum (black), spectral changes upon reduction (light red), and final spectrum (red). (C) Schematic representation of the reactivity observed by FTIR-SEC under CO_2.

that the new signals could correspond to the neutral [Mn(H)-$(CO)_3$(bis-^{Me}NHC)] complex (**1-H**).[6f,10a,11a,15,16]

Chemical Synthesis and Characterization of the Mn(I) Hydride [Mn(H)$(CO)_3$(bis-^{Me}NHC)] (1-H). To further investigate the nature of the latter species, the chemical reduction of **1-MeCN**$^+$ was attempted (see the SI). After stirring for 2 h an anhydrous MeCN solution (<40 ppm of H_2O) of **1-MeCN**$^+$ in the presence of Na/Hg amalgam excess, a bright orange solution was obtained, and an orange powder was isolated (33% yield). Notably, the FTIR spectrum of the solution matches the same spectral features observed during *in situ* FTIR-SEC (Figure 2A top, dashed blue trace). Interestingly, the X-ray analysis of single crystals obtained by slow diffusion of pentane into a toluene solution of the compound showed the formation of **1-H** (Figure 2C). The bond distances between the Mn and NHC or CO carbons are within the expected range (see the caption of Figure 2).

X-ray diffraction data collected for **1-H** single crystals suggest the presence of a H atom bound to the metal center, which is consistent with the charges in the geometry of the structure. Moreover, the ^{1}H NMR spectra in CD_3CN of the isolated crystals of **1-H** show a singlet signal at −6.88 ppm with an integral value of one, characteristic of a metal hydride (Figure 2D and Figure S5). The same signal was previously detected after reacting **1-MeCN**$^+$ with 2 equiv of $PhSiH_3$ in MeCN at 80 °C.[18] Under electrochemical conditions, the formation of **1-H** likely comes from the protonation of the transient highly nucleophilic **1**$^-$ anion by residual water traces contained in the solvent or by proton abstraction from MeCN. In addition, under electrochemical conditions, the electrolyte can also deliver protons *via* a Hofmann degradation.[19] Indeed, MeCN was previously reported as a suitable proton donor to low-valent metal complexes.[20] It is worth noting that such Mn−H species are also relevant for understanding the mechanism of several organic transformations catalyzed by **1-Br**. So far, it has also been postulated as a key intermediate in N-alkylation of anilines with alcohols,[21] ketone hydrosilylation,[18] and α-alkylation of ketones with alcohols.[22]

In agreement with the formation of a Mn(I) hydride species, FTIR-SEC data of **1-MeCN**$^+$ show a preferential formation of **1-H** in the presence of Brønsted acids. For instance, **1-H** is predominantly formed by reducing **1-MeCN**$^+$ in aqueous MeCN (0.2 M H_2O, Figure S15), and the intensity of its spectral features increases upon increasing the water concentration (1 M, Figure S16). Furthermore, FTIR-SEC displays a complete conversion of **1-MeCN**$^+$ into **1-H** with isosbestic points in the presence of stronger Brønsted acids (0.02 M PhOH) (Figure 2A, blue trace). The negative absorbance values at 1607 and 1595 cm^{-1} account for the PhOH consumption during the process, whereas the growth of a broad band at 1583 cm^{-1} indicates the concomitant phenoxide base (PhO^-) formation.[23]

Complex **1-H** could also be quantitatively formed by bulk electrolysis at −2.28 V of a **1-MeCN**$^+$ solution containing 0.02 M PhOH under Ar (Figure S17), suggesting good electrochemical stability of **1-H** under these conditions. Voltammetric data of **1-MeCN**$^+$ in MeCN show a negligible increase of the reductive peak current up to *ca.* 0.5 M of added water (Figure S18). A slight current increase is observed only at higher [H_2O] and high overpotentials. Moreover, it is worth noting that the CV of **1-H** in anhydrous MeCN does not show any observable reduction peaks over a wide potential window (Figure S20), in agreement with the extremely reducing DFT-calculated redox potential for this species (−4.23 V). The extended stability of **1-H** contrasts the pronounced instability reported for the analogous Mn−H species with polypyridyl ligands and provides a unique opportunity to study the stoichiometric reactivity of the isolated complex (see below).

Electrocatalytic CO_2 Reduction Mediated by 1-MeCN$^+$ in Anhydrous MeCN. In the CV under a CO_2-saturated atmosphere, a dramatic current increase is observed at the reduction wave of **1-MeCN**$^+$, indicating a fast electrocatalytic CO_2 reduction process (Figure 3A). The catalytic wave shows an onset potential at −2.07 V and an S-shaped plateau at −2.54 V. The analysis of the CVs at increasing scan rates results in an estimated $TOF_{max} = (3.0 \pm 0.2) \times 10^3$ s^{-1}, slightly higher than that previously reported for **1-Br** under the same conditions (Figure S21, see the SI).[17a] The catalytic current was first-order in catalyst concentration (Figure S22). Controlled-potential electrolysis (CPE) of **1-MeCN**$^+$ under CO_2 resulted in a stable catalytic CO production with excellent selectivity (FE_{CO} of ~90%) for more than 5 h (Table S1 and Figures S23 and S24).

No hydrogen was detected during the experiments, whereas minor traces of formate accounting for *ca.* 0.1% FE were found by ^{1}H NMR analysis of the electrolyzed solution after several hours of reaction (Figure S25).

We also carried out thin-layer FTIR-SEC studies to gain information about the catalytic reaction. At an applied potential of *ca.* −2.1 V, the rapid growth of IR bands at 1684 and 1645 cm^{-1} indicates the formation of free HCO_3^-/CO_3^{2-} species typically associated with the electrocatalytic CO_2-to-CO conversion process in aprotic media (Figure 3B).[10a,24] At the same time, the growing ν_{CO} bands at 2090, 2002, and 1969 cm^{-1} indicate the formation of a new carbonyl species (Figure 3B). This species, previously detected during FTIR-SEC of **1-Br**, was assigned to the tetracarbonyl intermediate $[Mn(CO)_4(bis\text{-}^{Me}NHC)]^+$ (**1-CO$^+$**).[9d] The formation of structurally similar complexes under CO_2RR conditions was also reported for other Mn-based catalysts with bis-NHC or polypyridyl ligands.[15,17d] It should also be emphasized that the lack of detection of the **1**$^-$ bands during FTIR-SEC under CO_2 is consistent with its fast reactivity with CO_2 to form **1-CO$^+$**. The latter is apparently the only accumulated intermediate during CO_2RR, thus representing the resting state under these conditions.

To further confirm the identity of **1-CO$^+$**, we synthesized a fresh sample of the compound by bubbling CO (1 atm) into a solution of **1-MeCN$^+$** in a noncoordinating solvent ($CHCl_3$ or CH_2Cl_2, Figure 4A, see the SI). The reaction was monitored

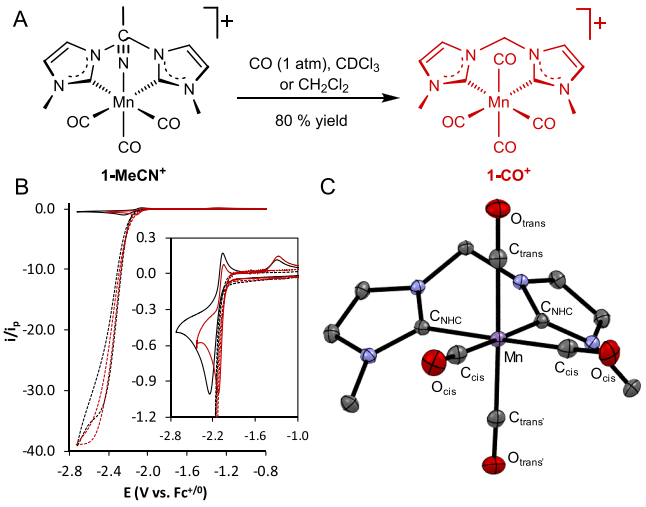

Figure 4. (A) Chemical generation of **1-CO$^+$**. (B) CVs of **1-MeCN$^+$** (black) and **1-CO$^+$** (red) under Ar (solid trace) and CO_2 (dashed trace). Scan rate = 100 mV s^{-1}. (C) ORTEP structure of **1-CO$^+$** obtained by single-crystal XRD. Relevant bond distances (in Å): $d(Mn-C_{trans})$ = 1.8377(17); $d(Mn-C_{trans'})$ = −1.8743(17); $d(Mn-C_{cis})$ = 1.8416(12); $d(Mn-C_{NHC})$ = 2.0441(11)−2.0442(11); $d(C_{cis}-O_{cis})$ = 1.1400(15); $d(C_{trans}-O_{trans})$ = 1.141(2); $d(C_{trans'}-O_{trans'})$ = 1.135(2).

over time by FTIR (Figure S26) and ^{1}H NMR (Figure S27), showing a complete conversion of **1-MeCN$^+$** into **1-CO$^+$** in approximately one hour at room temperature under CO saturation. The slow kinetics for **1-CO$^+$** formation from **1-MeCN$^+$**, compared with the fast catalytic rate, indicates that **1-CO$^+$** is formed within the catalytic cycle and not from the coordination of the catalytically formed CO to **1-MeCN$^+$**. The FTIR spectrum of the as-synthesized **1-CO$^+$** sample in MeCN matches the spectral features in the FTIR-SEC experiments of **1-MeCN$^+$** under CO_2 (Figure 3B). X-ray diffraction analysis of suitable crystals confirmed the formation of the Mn(I) tetracarbonyl **1-CO$^+$** complex (Figure 4C).

The voltammetric profile of **1-CO$^+$** under Ar exhibits an irreversible reduction peak at −2.12 V, occurring *ca.* 120 mV more positively than the peak potential of **1-MeCN$^+$** (Figure 4B and Figure S20). Furthermore, the lack of detection of the neutral $[Mn(CO)_4(bis\text{-}^{Me}NHC)]^0$ complex during FTIR-SEC of **1-CO$^+$** suggests a fast CO dissociation upon reduction of **1-CO$^+$** (Figure S29). Similar behavior has been recently shown for a Mn tetracarbonyl bpy-based complex.[25] Importantly, the **1-CO$^+$** complex acts as a precatalyst for efficient CO_2 electroreduction, displaying an analogous S-shaped catalytic voltammetric wave to that of **1-MeCN$^+$** (Figure 4B and Figure S30) and a similar TOF_{max} value $(3.2 \pm 0.2) \times 10^3$ s^{-1} (Figure S31). These results also indicate that **1-CO$^+$** is an on-cycle intermediate in the protonation-first mechanism for CO_2RR to CO catalyzed by **1-MeCN$^+$**.

Electrocatalytic CO_2 Reduction in the Presence of Brønsted Acids. The addition of small amounts of water strongly boosts the catalytic CO_2RR response of **1-MeCN$^+$**, with a maximum rate of $TOF_{max} = (3.94 \pm 0.04) \times 10^5$ s^{-1} for $[H_2O]$ ~ 0.5 M (Figures S32 and S33). Electrolysis data show an excellent selectivity toward CO production (−2.65 V, 5 h, FE_{CO} = 90%, Figure S34 and Table S1). No H_2 was detected in the gas phase, whereas a small but non-negligible amount of formate was detected by ^{1}H NMR, accounting for *ca.* 4% FE (Figure S34E). Further addition of water ($[H_2O]$ > 0.5 M) leads to a striking drop in catalytic current under CO_2 (Figure S35). This behavior is consistent with the chronoamperometric experiments at −2.65 V in 2 M H_2O, which reveal a drastic decrease in catalyst CO_2RR activity and selectivity (Table S1 and Figure S36). Under these conditions, FE for CO production was 66%, with a concomitant increase of the H_2 evolution (FE_{H2} = 28%) and formate production (FE_{HCOO-} = 7%, Figure S36C). The quantitative data show an increase of FE for H_2 and $HCOO^-$ formation over CO upon increasing the proton concentration in solution.

FTIR-SEC was used to explore the reactivity of the electrogenerated species toward CO_2 during the catalytic reaction in the presence of external proton sources. In a CO_2-saturated aqueous MeCN electrolyte (0.2 M H_2O), **1-MeCN$^+$** rapidly converts into **1-CO$^+$** as the predominant species when the applied potential reaches the foot of the catalytic wave (*ca.* −2.1 V, Figure S37A), as previously seen in anhydrous conditions (Figure 3B). Although the formation of **1-H** is highly favored under an Ar atmosphere (Figure S15), **1-H** is not observed when the solution is CO_2-saturated. These results emphasize the excellent selectivity of **1-MeCN$^+$** for CO_2-to-CO reduction over hydrogen evolution reaction (HER) at the low $[H_2O]$ regime. Remarkably, even with moderate amounts of water, the CO_2 binding to **1**$^-$ is faster than the protonation of the Mn center.

By holding the applied potential at *ca.* −2.1 V for a few minutes, further CO_2 consumption in the OTTLE cell[26] (~60% of the initial concentration) is accompanied by a slow increase of new ν_{CO} stretches (2008, 1920, and 1880 cm^{-1}) at the expense of **1-CO$^+$**. A clear competitive formation of a new *fac*-tricarbonyl Mn species is observed (Figure S37B). But notably, FTIR-SEC in the presence of stronger Brønsted acids (PhOH 0.02 M) displays an enhanced formation of new species (Figure 5C), likely corresponding to the transient **1-H** and the neutral $[Mn(CO)_3(bis\text{-}^{Me}NHC)(OCOH)]$ complex (**1-OCOH**), as

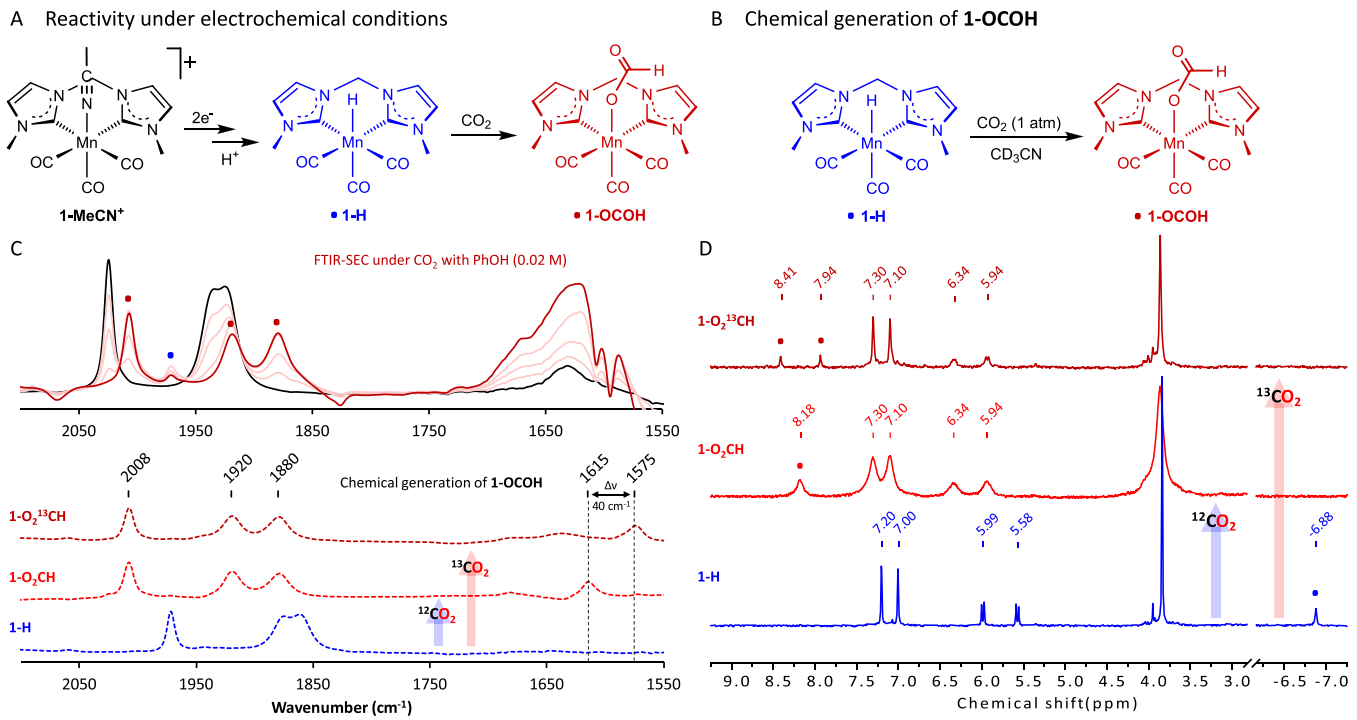

Figure 5. (A) Schematic representation of the reactivity of **1-MeCN**$^+$ observed by FTIR-SEC under CO_2 with PhOH. (B) Scheme of the chemical generation of **1-OCOH**. (C) FTIR-SEC of **1-MeCN**$^+$ (4 mM) in 0.2 M $TBAPF_6$/MeCN with added PhOH (0.02 M) under CO_2, starting spectrum (black), spectral changes upon reduction (light red), and final spectrum (red). FTIR spectra of **1-H**, **1-OCOH**, and **1-O^{13}COH** in MeCN solution (dashed traces). (D) ^{1}H NMR (400 MHz, CD_3CN) of **1-H**, **1-OCOH**, and **1-O^{13}COH**.

confirmed by direct comparison with the IR spectrum of an authentic synthesized sample of **1-OCOH** by the reaction of **1-MeCN**$^+$ with an excess of tetrabutylammonium formate (Figure S38, see the SI). Although other related Mn−formate complexes with diimine or PNP pincer ligands have been previously reported,[16,27] this is a rare direct experimental piece of evidence of a metal-formate adduct formed during CO_2 electroreduction catalyzed by a molecular complex.[28] It can be rationalized that the **1-OCOH** intermediate originates from the reaction between CO_2 and the transient **1-H**. As shown above, **1-H** is quantitatively electrogenerated under Ar in the presence of 0.02 M PhOH (Figure 2A). However, difficult detection of **1-H** during FTIR-SEC under CO_2 suggests that the reaction with CO_2 is fast. This was further corroborated by the reactivity of the chemically synthesized **1-H** complex with CO_2.

The CO_2 bubbling into a solution of **1-H** results in a quantitative formation of **1-OCOH** (Figure 5B). The FTIR spectrum of the as-synthesized complex matches that obtained during FTIR-SEC under CO_2 with 0.02 M PhOH (Figure 5C). The ^{1}H NMR characterization is also consistent with the formation of a Mn−formate complex, as indicated by the complete disappearance of the hydride resonance at −6.88 ppm and the growth of a singlet at 8.19 ppm, characteristic of the formate ligand proton (Figure 5D). Both, FTIR and ^{1}H NMR results are consistent with a *fac*-Mn(bis-^{Me}NHC)$(CO)_3$ formate complex. Moreover, $^{13}CO_2$ labeling experiments unambiguously confirmed the reactivity of the Mn−H with CO_2 at room temperature. A 40 cm^{-1} isotopic shift is observed for the formate ν_{C-O} stretches (1615 cm^{-1} under $^{12}CO_2$ and 1575 cm^{-1} under $^{13}CO_2$, Figure 5C).[29] Further experimental proofs were provided by ^{1}H and ^{13}C NMR, with the coordinated $H^{13}CO_2^-$ ligand appearing as a doublet centered at 8.18 ppm in the ^{1}H NMR spectrum (J_{13C-Hf} = 191.1 Hz, see Figure 5D).

The electrolysis data under protic conditions (Table S1) show low overall turnover numbers and FE values for catalytic CO_2 reduction to $HCOO^-$, compared to the competitive CO production. Further efforts to increase the efficiency of $HCOO^-$ production by adding Brønsted acids stronger than water (0.02 M PhOH) resulted in only a slight increase of FE_{HCOO^-} (15%) but also in a significant drop of catalytic current.

As previously discussed for **1-CO**$^+$, the observation of **1-OCOH** as a stable intermediate implies an unfavorable $HCOO^-$ dissociation (*vide infra*), and a further reduction step is required to promote the $HCOO^-$ dissociation. Compared to **1-CO**$^+$, the peak potential of the neutral **1-OCOH** complex occurs *ca.* 500 mV more negatively (Figures S20 and S30). Therefore, we propose that the observed CO_2RR efficiency and selectivity are mainly determined by the different kinetics of the **1**$^-$ protonation *versus* CO_2 coordination steps and by the reduction potentials of **1-CO**$^+$ *versus* **1-OCOH**. To corroborate our hypothesis, we investigated the two competitive CO_2 reduction pathways by computational modeling.

Mechanistic Discussion Based on DFT Calculations. We have computed the proton-assisted CO production pathway and the formate production mechanism, including the protonation of the anionic intermediate (**1**$^-$) to give **1-H**, by considering H_2O (or PhOH) as added Brønsted acids to shed light on the fundamental steps governing the catalytic activity and selectivity. Previous reports in the field have shown that the hybrid functional B3LYP successfully supported experimental data including structural, spectroscopic, and reactivity studies in related Mn−tricarbonyl catalysts.[13,30] The different intermediate and transition state (TS) structures were obtained after geometry optimization at their low spin configuration followed by frequency analysis at the B3LYP-D_3/6-311++G(d,p) level of theory unless otherwise indicated. Then, the electronic energies

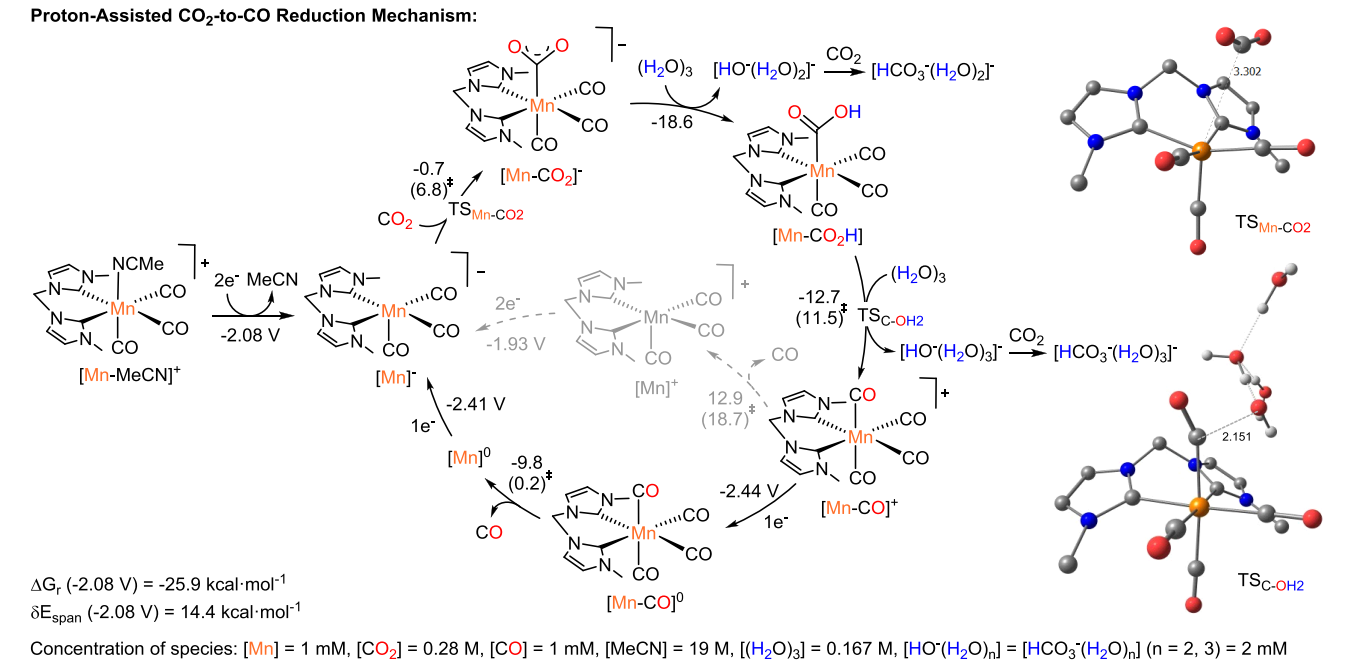

Figure 6. Computed proton-assisted CO_2-to-CO reduction catalytic cycle at the B3LYP-D_3/6311++G(d,p)//B3LYP-D_3/6-311++G(2d,2p) level of theory with relevant optimized TS structures. Redox potentials in V vs $Fc^{+/0}$ and Gibbs free energies in kcal·mol^{-1} (barriers in parenthesis).

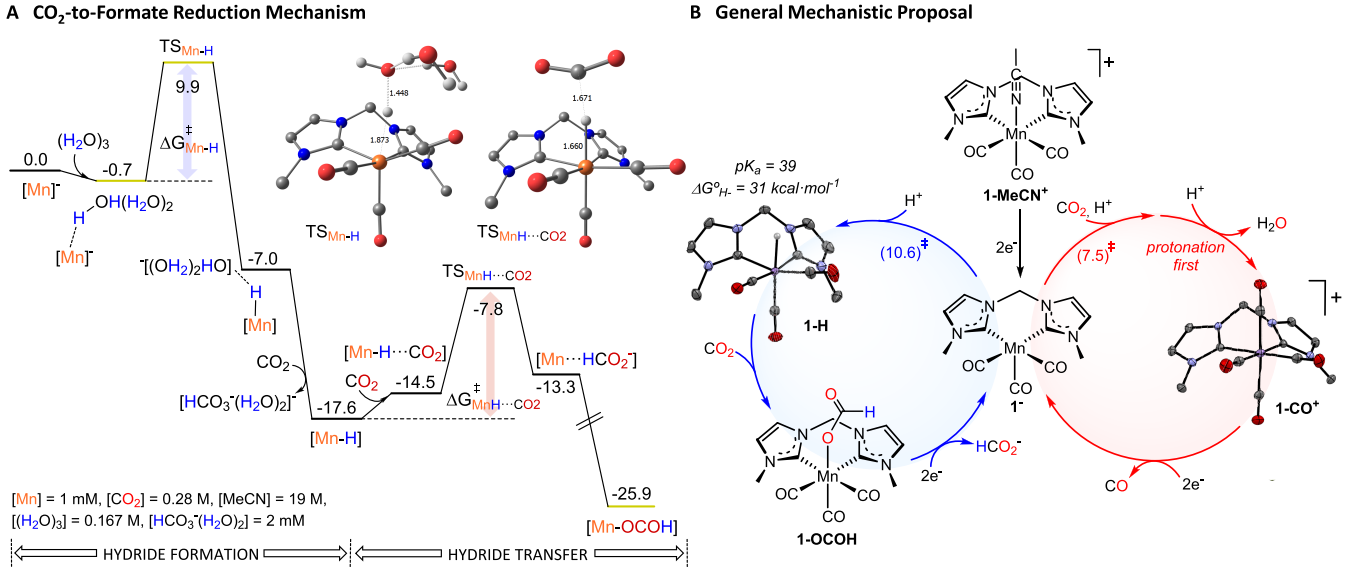

Figure 7. (A) Gibbs energy (kcal·mol^{-1}) profile of the CO_2 reduction to formate mechanism calculated at the B3LYP-D_3/6-311++G(d,p)//B3LYP-D_3/6-311++G(2d,2p) level of theory. (B) General mechanistic proposal for the CO_2 reduction to CO (red) and formate (blue) catalyzed by **1-MeCN**$^+$. Gibbs energy barriers (kcal·mol^{-1}) are shown in parentheses.

were computed at the B3LYP-D_3/6-311++G(2d,2p) level for a more accurate description of the thermodynamics, and solvent effects were considered through the implicit SMD model for acetonitrile. In the steps where protons are transferred, explicit solvent molecules have been included to better describe the effective acidity of the proton donor as well as the stabilization of the resulting conjugate base by hydrogen bonding. Further details on the computational methodology can be found in the SI.

Proton-Assisted CO_2-to-CO Reduction Mechanism. The highly nucleophilic $[Mn]^-$ intermediate can be formed *via* an overall 2e$^-$ reduction of the starting complex $[Mn{-}MeCN]^+$ at a computed reduction potential of −2.08 V (Figure 6 and Scheme S2). As depicted in Figure 6, the CO_2 binding to $[Mn]^-$ is slightly exergonic and takes places through a 6.8 kcal·mol^{-1} transition state (TS_{Mn-CO_2}). Then, following the protonation-first mechanism, the C−O bond cleavage occurs after the double protonation of the former carboxylate intermediate. Assuming a water cluster concentration $[(H_2O)_3]$ of 0.167 M, the formation of the complex-$[(H_2O)_3]$ adduct is exergonic by −4.2 kcal·mol^{-1}, whereas the first proton transfer step is slightly endergonic. However, the formation of $[Mn{-}CO_2H]$ becomes exergonic when the thermodynamics of the hydrogen carbonate formation from the generated OH^- is included in the energy profile. Then, the second protonation is also exergonic and proceeds through a kinetic barrier of 11.5 kcal·mol^{-1} to form

Mn−CO$^+$. In this process, one H_2O molecule and two solvated HCO_3^- are released. Once the C−O bond is cleaved, the resulting Mn-bound CO should be released to recover the catalytically active species.

The CO release from [Mn−CO]$^+$ to give the 16e$^-$ [Mn]$^+$ species is endergonic by 12.9 kcal·mol^{-1}, and the kinetic barrier for this step is 18.7 kcal·mol^{-1}. Instead, at −2.08 V, the electrochemically driven CO release to give the corresponding 17e$^-$ species [Mn]^0 is exergonic and presents a lower kinetic barrier (8.5 kcal·mol^{-1}). Finally, the turnover of the catalytic cycle takes place upon the recovery of the reduced species [Mn$^-$]. Under these conditions, the energy span (δE_{span}) of the most favorable catalytic pathway is 14.4 kcal·mol^{-1}, which accounts for the kinetics of CO_2 binding ($\Delta G^{\ddagger}_{CO2}$ = 6.8 kcal·mol^{-1}) and the reduction of [Mn]^0 to [Mn]$^-$ (Figure S40). Although our DFT calculations predict that [Mn−CO]$^+$, *i.e.*, the species experimentally characterized as the resting state, is 1.5 kcal·mol^{-1} higher in energy than [Mn]^0, this small energy difference is below the usual DFT accuracy, which is usually higher in the comparison of species with a different net charge. It is worth noting that, at more negative potentials (< −2.41 V), the energy span is only determined by the C−O bond cleavage step (δE_{span} = $\Delta G^{\ddagger}_{C-OH2}$ = 11.5 kcal·mol^{-1}). Therefore, the reaction rate becomes redox-independent at high overpotential, which aligns with the high current observed in the CV and the plateau-shaped voltammogram obtained at high scan rates (Figures S21 and S31).

Mechanism of the CO_2 Reduction to Formate. In a previous section, we showed that **1-H** could be formed by protonating the anionic **1**$^-$ intermediate. As shown in the Gibbs energy profile in Figure 7A, we have computationally studied the formation mechanism of **1-H** from **1-MeCN**$^+$ and the subsequent proton transfer step by modeling a cluster of three water molecules, as in the CO_2-to-CO reduction mechanism (Figure 6). The difference between the kinetic barrier modeled with a three- and a four-membered water cluster is less than one kcal·mol^{-1} within the error of the DFT method (Figure S42). For this reason, we have modeled the CO_2-to-formate reduction energy profile considering a cluster of three water molecules (Figure 7A). In this mechanism, the protonation of the [Mn]$^-$ intermediate is exergonic by 17.6 kcal·mol^{-1} with an associated kinetic barrier for the hydride formation ($\Delta G^{\ddagger}_{Mn-H}$) of 10.6 kcal·mol^{-1}. The subsequent step corresponds to the exergonic hydride transfer to the CO_2 molecule to forge the H−C bond of the formate anion. The kinetic barrier of the hydride transfer step ($\Delta G^{\ddagger}_{MnH\cdots CO2}$) is 9.8 kcal·mol^{-1}, in agreement with the kinetic barrier obtained for the same step with the analogous Mn−bpy complex (10.1 kcal·mol^{-1}).[13] This step ultimately results in the formation of [Mn−OCOH], which is 25.9 kcal·mol^{-1} more stable than the [Mn]$^-$ species. These results confirm that the Mn(I) formate intermediate is thermodynamically and kinetically accessible at room temperature starting from **1-MeCN**$^+$ under CO_2 electroreduction conditions in wet acetonitrile.

General Mechanistic Discussion. After gathering the experiments and computational results, we present a general mechanistic picture merging the CO_2 reduction cycles to CO and formate (Figure 7B). In aprotic conditions or in the presence of moderate amounts (≤0.5 M) of added H_2O, the CO_2RR proceeds preferably through the CO_2-to-CO pathway producing almost solely CO with excellent efficiencies. The detection of **1-CO**$^+$ under *in situ* electrocatalytic conditions indicates that the CO_2 reduction to CO occurs through a protonation-first mechanism. At the redox potential of **1-MeCN**$^+$ to **1**$^-$, **1-CO**$^+$ is the resting state of the reaction, requiring a 1e$^-$ reduction step to undergo CO release. In this regard, the **1-CO**$^+$ species is reduced at more positive potentials than **1-MeCN**$^+$ (Figure 4B and Figure S20), leading to an energetically favored proton-assisted mechanism for CO_2-to-CO conversion.

In the presence of added protons, a competitive protonation of the **1**$^-$ anion leads to the formation of a Mn−H species, **1-H**. The pK_a value of **1-H** was extrapolated by using a linear pK_a *versus* the redox potential correlation (see SI, Scheme S1).[31] The estimated pK_a (39.3 ± 1.0) for **1-H** is considerably higher than those reported for the polypyridyl counterparts and supports the observation of a fast **1**$^-$ protonation in MeCN (Figure 7B).[32] Then, **1-H** has shown a rapid hydride transfer to the CO_2 molecule giving the corresponding Mn formato complex (**1-OCOH**). Three main factors are crucial to rationalize the CO_2 electroreduction reactivity and selectivity of the **1**$^-$ catalyst:

Hydricity of 1-H. The hydricity of a metal hydride, ΔG^0_{H-}, describes the thermodynamic hydride donor character and is commonly used to predict the capability of a metal hydride to undergo a hydride transfer to CO_2 to form HCOO$^-$.[31a] By using a linear correlation recently found between ΔG^0_{H-} and the redox potential of the parent complex across a series of several transition metal hydrides,[31b] we estimated a ΔG^0_{H-} of 31.4 ± 2.0 kcal·mol^{-1} for **1-H** (see the SI). The estimated ΔG^0_{H-} of **1-H** is significantly lower than the values reported for structurally similar Mn(I) hydrides containing bipyridyl ligands used for CO_2RR to HCOO$^-$ (Table S3 and Figure S39),[16] thus indicating a much stronger hydride donor ability, which reflects the increased σ-donor properties of the bis-^{Me}NHC moiety. In particular, since the hydricity of formate in MeCN is 44 kcal·mol^{-1},[31a] the hydride transfer to CO_2 to form HCOO$^-$ is predicted to be exergonic by 12.6 kcal·mol^{-1} for **1-H**. For the manganese bipyridyl complexes shown in Figure S39, the authors claim that this process becomes energetically favorable if the formate binding to Mn(I) is considered.[16] In the case of an amine-functionalized bipyridyl Mn catalyst, access to the more hydridic reduced form of the Mn(I) hydride intermediate is required to observe an efficient CO_2-to-formic acid process.[6f]

Stability of the Metal-Formate Intermediate. Despite the energetically favored formation of the **1-OCOH** intermediate in protic media under a CO_2 atmosphere (Figure 7A), the rate and efficiency of the electrocatalytic CO_2RR to HCOO$^-$ obtained during electrolysis are low compared to the competitive pathway leading to CO. Therefore, other thermodynamic and kinetic factors need to be considered to explain the product distribution observed under catalytic conditions. A main concern from the thermodynamic point of view is the HCOO$^-$ dissociation step from a neutral metal-formate complex. For some Ru systems employed for CO_2 conversion to formate, an efficient HCOO$^-$ release was reported only after reducing the neutral formate complex.[28,33] For a bipyridyl Mn(I) catalyst with pendant amines, the HCOO$^-$ liberation is proposed to take place from an anionic species formed upon one-electron reduction of the neutral Mn(I) formate intermediate.[6f] In the case of our bis-NHC Mn(I) system, the stability of the **1-OCOH** intermediate generated under SEC conditions suggests that an additional reduction step is required to promote the release of HCOO$^-$; likewise, it is necessarily a 1e$^-$ reduction of **1-CO**$^+$ to release CO in the protonation-first mechanism. Nevertheless, the reduction of **1-OCOH** takes place at considerably more negative potentials than **1-CO**$^+$ (*ca.* 450 mV), implying that the catalytic CO_2-to-HCOO$^-$ requires a larger overpotential to occur. Therefore, the

remarkable difference between the redox potentials of the pivotal **1-OCOH** and **1-CO**$^+$ intermediates primarily determine the preferential selectivity toward CO production over $HCOO^-$ formation observed during CO_2 electroreduction in the presence of Brønsted acids.

*Competitive Kinetics of Protonation versus CO_2 Binding to the Key Anionic **1**$^-$ Species.* In this regard, our experimental data show that **1**$^-$ is an extremely CO-selective catalyst, suggesting that CO_2 binding is favored over metal protonation at the explored conditions. In line with the experiments, the direct comparison between the DFT-calculated energy profiles leading to CO and HCO_2^- formation (Figures S43 and S44) indicates that the CO_2 binding step to the $[Mn]^-$ active species has a lower Gibbs energy barrier ($\Delta G^{\ddagger}_{Mn-CO2}$ = 7.5 kcal·mol^{-1}) than the protonation of the metal to form the [Mn−H] intermediate ($\Delta G^{\ddagger}_{Mn-H}$ = 10.6 kcal·mol^{-1}). Nevertheless, other factors such as substrate transfer processes (H^+ *vs* CO_2 diffusion) play a crucial role in determining the overall kinetics of both the processes.

CONCLUSIONS

In this work, we have elucidated the electrochemical CO_2RR mechanism catalyzed by the highly active *fac*-$[Mn^I(CO)_3$(bis-^{Me}NHC)MeCN$]^+$ (**1-MeCN**$^+$) complex in neat acetonitrile as well as in the presence of Brønsted acids. Competitive pathways leading to CO and $HCOO^-$ formation are operative, depending on the applied potential and the concentration of protons in solution. In particular, the activity and selectivity of the **1-MeCN**$^+$ precatalyst depend on the interplay of the three main intermediate species in the catalytic cycles, *i.e.*, **1-CO**$^+$, **1-H**, and **1-OCOH**, which are thoroughly characterized by a combination of organometallic reactivity studies, electrochemistry, spectroelectrochemistry, and DFT calculations. In anhydrous MeCN or in the presence of a moderate amount of water (≤0.5 M), record catalytic rates and selectivity for CO production were observed due to an extremely fast CO_2 binding to the electrogenerated **1**$^-$ active catalyst. This process occurs through a protonation-first mechanism, as corroborated by the unambiguous identification of the tetracarbonyl **1-CO**$^+$ species.

In addition to the main CO_2-to-CO mechanism, we have identified a competitive pathway leading to electrocatalytic formate production, favored when increasing the proton concentration in solution. The origin of the observed formate production was ascribed to the protonation of **1**$^-$ to generate the Mn(I) hydride **1-H** species, detected as the main intermediate by FTIR-SEC in the absence of CO_2. This species was independently isolated and fully characterized, affording the first X-ray structure of a Mn−H in the context of electrocatalytic CO_2RR with *fac*-Mn$(CO)_3$ complexes. Furthermore, we have demonstrated the mechanistic relevance of **1-H** in the CO_2-to-formate reduction pathway showing an extremely fast reactivity of the latter with CO_2 to give the corresponding neutral Mn−formate species (**1-OCOH**). This was confirmed by combining SEC, organometallic reactivity studies (including labeling experiments under $^{13}CO_2$), computational modeling, and thermochemical analysis. However, although the **1-OCOH** formation is thermodynamically favored with moderate amounts of added water, its high stability limits the catalytic formate production. Both competing **1-CO**$^+$ and **1-OCOH** intermediates require an electrochemical step to promote product release, but the latter requires a considerably larger overpotential than the former (difference of *ca.* 450 mV). Moreover, the kinetics of the competitive CO_2 binding *vs* protonation of the anionic **1**$^-$ catalyst is crucial to determine the CO_2 electroreduction activity and selectivity. Overall, our experimental and computational results support the preferential selectivity of **1**$^-$ for CO over formate production under CO_2, emphasizing the extremely high intrinsic selectivity of **1**$^-$ toward CO_2RR and the importance of the $HCOO^-$ release step for an efficient CO_2-to-formate electroreduction. The compelling set of mechanistic evidence presented in this work will help to rationalize and control the product selectivity in the electrochemical CO_2RR catalyzed by molecular systems.

ASSOCIATED CONTENT

Supporting Information

The Supporting Information is available free of charge at https://pubs.acs.org/doi/10.1021/acscatal.3c01430.

General methods and materials, synthesis and characterization of complexes, electrochemistry, SEC, estimation of thermodynamic parameters, and computational details with optimized DFT structures (PDF)

Crystallographic information of [**1-CO**]BF_4 (CIF)

Crystallographic information of **1-H** (CIF)

Crystallographic information of **1-Br** (CIF)

AUTHOR INFORMATION

Corresponding Authors

Federico Franco − *Institute of Chemical Research of Catalonia (ICIQ), The Barcelona Institute of Science and Technology, 43007 Tarragona, Spain*; Email: ffranco@iciq.es

Josep M. Luis − *Institut de Química Computacional i Catèlisi (IQCC) and Departament de Química, Universitat de Girona, Campus Montilivi, Girona E-17003 Catalonia, Spain*; orcid.org/0000-0002-2880-8680; Email: josepm.luis@udg.edu

Julio Lloret-Fillol − *Institute of Chemical Research of Catalonia (ICIQ), The Barcelona Institute of Science and Technology, 43007 Tarragona, Spain; Catalan Institution for Research and Advanced Studies (ICREA), 08010 Barcelona, Spain*; orcid.org/0000-0002-4240-9512; Email: jlloret@iciq.es

Authors

Sergio Fernández − *Institute of Chemical Research of Catalonia (ICIQ), The Barcelona Institute of Science and Technology, 43007 Tarragona, Spain*; orcid.org/0000-0002-1620-8514

Marta Martínez Belmonte − *Institute of Chemical Research of Catalonia (ICIQ), The Barcelona Institute of Science and Technology, 43007 Tarragona, Spain*

Sofia Friães − *Instituto de Tecnologia Química e Biológica António Xavier (ITQB), Nova University of Lisbon, 2780-157 Oeiras, Portugal*

Beatriz Royo − *Instituto de Tecnologia Química e Biológica António Xavier (ITQB), Nova University of Lisbon, 2780-157 Oeiras, Portugal*; orcid.org/0000-0002-7909-9992

Complete contact information is available at: https://pubs.acs.org/10.1021/acscatal.3c01430

Notes

The authors declare no competing financial interest.

■ ACKNOWLEDGMENTS

The authors acknowledge financial support from the ICIQ Foundation, the CERCA Program/Generalitat de Catalunya, MICINN through Severo Ochoa Excellence Accreditation 2020-2023 (CEX2019-000925-S, MIC/AEI), the European Research Foundation for H2020 project ERC-2015-CoG GREENLIGHT_REDCAT 648304, (J.L.-F.), the Spanish Ministry of Universities for an FPU fellowship FPU16/04234 (S.F.), AGAUR (2017-SGR-1647, J.L.-F.; 2017SGR39, J.M.L.), and MICINN (PID2019-110050RB-I00, J.L-F.; PGC2018-098212-B-C22, J.M.L.).

■ REFERENCES

(1) (a) Franco, F.; Rettenmaier, C.; Jeon, H. S.; Roldan Cuenya, B. Transition metal-based catalysts for the electrochemical CO_2 reduction: from atoms and molecules to nanostructured materials. *Chem. Soc. Rev.* **2020**, *49*, 6884−6946. (b) Perry, S. C.; Leung, P.-K.; Wang, L.; Ponce de León, C. Developments on carbon dioxide reduction: Their promise, achievements, and challenges. *Curr. Opin. Electrochem.* **2020**, *20*, 88−98. (c) Navarro-Jaén, S.; Virginie, M.; Bonin, J.; Robert, M.; Wojcieszak, R.; Khodakov, A. Y. Highlights and challenges in the selective reduction of carbon dioxide to methanol. *Nat. Rev. Chem.* **2021**, *5*, 564−579. (d) Saha, P.; Amanullah, S.; Dey, A. Selectivity in Electrochemical CO_2 Reduction. *Acc. Chem. Res.* **2022**, *55*, 134−144.

(2) Kibria, M. G.; Edwards, J. P.; Gabardo, C. M.; Dinh, C.-T.; Seifitokaldani, A.; Sinton, D.; Sargent, E. H. Electrochemical CO_2 Reduction into Chemical Feedstocks: From Mechanistic Electrocatalysis Models to System Design. *Adv. Mater.* **2019**, *31*, 1807166.

(3) (a) Kaim, W.; Fiedler, J. Spectroelectrochemistry: the best of two worlds. *Chem. Soc. Rev.* **2009**, *38*, 3373−3382. (b) Machan, C. W.; Sampson, M. D.; Chabolla, S. A.; Dang, T.; Kubiak, C. P. Developing a Mechanistic Understanding of Molecular Electrocatalysts for CO_2 Reduction using Infrared Spectroelectrochemistry. *Organometallics* **2014**, *33*, 4550−4559. (c) Rosser, T. E.; Reisner, E. Understanding Immobilized Molecular Catalysts for Fuel-Forming Reactions through UV/Vis Spectroelectrochemistry. *ACS Catal.* **2017**, *7*, 3131−3141.

(4) (a) Boutin, E.; Merakeb, L.; Ma, B.; Boudy, B.; Wang, M.; Bonin, J.; Anxolabéhère-Mallart, E.; Robert, M. Molecular catalysis of CO_2 reduction: recent advances and perspectives in electrochemical and light-driven processes with selected Fe, Ni and Co aza macrocyclic and polypyridine complexes. *Chem. Soc. Rev.* **2020**, *49*, 5772−5809. (b) Kinzel, N. W.; Werlé, C.; Leitner, W. Transition Metal Complexes as Catalysts for the Electroconversion of CO_2: An Organometallic Perspective. *Angew. Chem., Int. Ed.* **2021**, *60*, 11628−11686. (c) Francke, R.; Schille, B.; Roemelt, M. Homogeneously Catalyzed Electroreduction of Carbon Dioxide—Methods, Mechanisms, and Catalysts. *Chem. Rev.* **2018**, *118*, 4631−4701. (d) Franco, F.; Fernández, S.; Lloret-Fillol, J. Advances in the electrochemical catalytic reduction of CO_2 with metal complexes. *Curr. Opin. Electrochem.* **2019**, *15*, 109−117. (e) Lense, S.; Grice, K. A.; Gillette, K.; Wolf, L. M.; Robertson, G.; McKeon, D.; Saucedo, C.; Carroll, P. J.; Gau, M. Effects of Tuning Intramolecular Proton Acidity on CO_2 Reduction by Mn Bipyridyl Species. *Organometallics* **2020**, *39*, 2425−2437.

(5) (a) Torbensen, K.; Boudy, B.; Joulié, D.; von Wolff, N.; Robert, M. Emergence of CO_2 electrolyzers including supported molecular catalysts. *Curr. Opin. Electrochem.* **2020**, *24*, 49−55. (b) Ren, S.; Joulié, D.; Salvatore, D.; Torbensen, K.; Wang, M.; Robert, M.; Berlinguette Curtis, P. Molecular electrocatalysts can mediate fast, selective CO_2 reduction in a flow cell. *Science* **2019**, *365*, 367−369. (c) Wang, M.; Torbensen, K.; Salvatore, D.; Ren, S.; Joulié, D.; Dumoulin, F.; Mendoza, D.; Lassalle-Kaiser, B.; Işci, U.; Berlinguette, C. P.; Robert, M. CO_2 electrochemical catalytic reduction with a highly active cobalt phthalocyanine. *Nat. Commun.* **2019**, *10*, 3602. ((d)) Fernández, S.; Dubed Bandomo, G. C.; Lloret-Fillol, J., Recent advances in electrocatalytic CO2 reduction with molecular complexes. In *Adv. Inorg. Chem.*, Academic Press: 2022.

(6) (a) Taheri, A.; Berben, L. A. Making C−H bonds with CO_2: production of formate by molecular electrocatalysts. *Chem. Commun.* **2016**, *52*, 1768−1777. (b) Kang, P.; Meyer, T. J.; Brookhart, M. Selective electrocatalytic reduction of carbon dioxide to formate by a water-soluble iridium pincer catalyst. *Chem. Sci.* **2013**, *4*, 3497−3502. (c) Kanega, R.; Onishi, N.; Wang, L.; Himeda, Y. Electroreduction of Carbon Dioxide to Formate by Homogeneous Ir Catalysts in Water. *ACS Catal.* **2018**, *8*, 11296−11301. (d) Taheri, A.; Thompson, E. J.; Fettinger, J. C.; Berben, L. A. An Iron Electrocatalyst for Selective Reduction of CO_2 to Formate in Water: Including Thermochemical Insights. *ACS Catal.* **2015**, *5*, 7140−7151. (e) Roy, S.; Sharma, B.; Pécaut, J.; Simon, P.; Fontecave, M.; Tran, P. D.; Derat, E.; Artero, V. Molecular Cobalt Complexes with Pendant Amines for Selective Electrocatalytic Reduction of Carbon Dioxide to Formic Acid. *J. Am. Chem. Soc.* **2017**, *139*, 3685−3696. (f) Rønne, M. H.; Cho, D.; Madsen, M. R.; Jakobsen, J. B.; Eom, S.; Escoudé, É.; Hammershøj, H. C. D.; Nielsen, D. U.; Pedersen, S. U.; Baik, M.-H.; Skrydstrup, T.; Daasbjerg, K. Ligand-Controlled Product Selectivity in Electrochemical Carbon Dioxide Reduction Using Manganese Bipyridine Catalysts. *J. Am. Chem. Soc.* **2020**, *142*, 4265−4275.

(7) Bourrez, M.; Molton, F.; Chardon-Noblat, S.; Deronzier, A. [Mn(bipyridyl)$(CO)_3$Br]: An Abundant Metal Carbonyl Complex as Efficient Electrocatalyst for CO_2 Reduction. *Angew. Chem., Int. Ed.* **2011**, *50*, 9903−9906.

(8) (a) Grills, D. C.; Ertem, M. Z.; McKinnon, M.; Ngo, K. T.; Rochford, J. Mechanistic aspects of CO_2 reduction catalysis with manganese-based molecular catalysts. *Coord. Chem. Rev.* **2018**, *374*, 173−217. (b) Stanbury, M.; Compain, J.-D.; Chardon-Noblat, S. Electro and photoreduction of CO_2 driven by manganese-carbonyl molecular catalysts. *Coord. Chem. Rev.* **2018**, *361*, 120−137.

(9) (a) Sampson, M. D.; Nguyen, A. D.; Grice, K. A.; Moore, C. E.; Rheingold, A. L.; Kubiak, C. P. Manganese Catalysts with Bulky Bipyridine Ligands for the Electrocatalytic Reduction of Carbon Dioxide: Eliminating Dimerization and Altering Catalysis. *J. Am. Chem. Soc.* **2014**, *136*, 5460−5471. (b) Yang, Y.; Ertem, M. Z.; Duan, L. An amide-based second coordination sphere promotes the dimer pathway of Mn-catalyzed CO_2-to-CO reduction at low overpotential. *Chem. Sci.* **2021**, *12*, 4779−4788. (c) Roy, S. S.; Talukdar, K.; Jurss, J. W. Electro- and Photochemical Reduction of CO_2 by Molecular Manganese Catalysts: Exploring the Positional Effect of Second-Sphere Hydrogen-Bond Donors. *ChemSusChem* **2021**, *14*, 662−670. (d) Ngo, K. T.; McKinnon, M.; Mahanti, B.; Narayanan, R.; Grills, D. C.; Ertem, M. Z.; Rochford, J. Turning on the Protonation-First Pathway for Electrocatalytic CO_2 Reduction by Manganese Bipyridyl Tricarbonyl Complexes. *J. Am. Chem. Soc.* **2017**, *139*, 2604−2618. (e) Sung, S.; Li, X.; Wolf, L. M.; Meeder, J. R.; Bhuvanesh, N. S.; Grice, K. A.; Panetier, J. A.; Nippe, M. Synergistic Effects of Imidazolium-Functionalization on fac-Mn$(CO)_3$ Bipyridine Catalyst Platforms for Electrocatalytic Carbon Dioxide Reduction. *J. Am. Chem. Soc.* **2019**, *141*, 6569−6582.

(10) (a) Franco, F.; Cometto, C.; Nencini, L.; Barolo, C.; Sordello, F.; Minero, C.; Fiedler, J.; Robert, M.; Gobetto, R.; Nervi, C. Local Proton Source in Electrocatalytic CO_2 Reduction with [Mn(bpy−R)$(CO)_3$Br] Complexes. *Chem. – Eur. J.* **2017**, *23*, 4782−4793. (b) Fokin, I.; Denisiuk, A.; Würtele, C.; Siewert, I. The Impact of a Proton Relay in Binuclear α-Diimine-Mn$(CO)_3$ Complexes on the CO_2 Reduction Catalysis. *Inorg. Chem.* **2019**, *58*, 10444−10453.

(11) (a) Reuillard, B.; Ly, K. H.; Rosser, T. E.; Kuehnel, M. F.; Zebger, I.; Reisner, E. Tuning Product Selectivity for Aqueous CO_2 Reduction with a Mn(bipyridine)-pyrene Catalyst Immobilized on a Carbon Nanotube Electrode. *J. Am. Chem. Soc.* **2017**, *139*, 14425−14435. (b) Dubed Bandomo, G. C.; Mondal, S. S.; Franco, F.; Bucci, A.; Martin-Diaconescu, V.; Ortuño, M. A.; van Langevelde, P. H.; Shafir, A.; López, N.; Lloret-Fillol, J. Mechanically Constrained Catalytic Mn$(CO)_3$Br Single Sites in a Two-Dimensional Covalent Organic Framework for CO_2 Electroreduction in H_2O. *ACS Catal.* **2021**, *11*, 7210−7222.

(12) (a) Takeda, H.; Koizumi, H.; Okamoto, K.; Ishitani, O. Photocatalytic CO_2 reduction using a Mn complex as a catalyst.

Chem. Commun. **2014**, *50*, 1491−1493. (b) Fei, H.; Sampson, M. D.; Lee, Y.; Kubiak, C. P.; Cohen, S. M. Photocatalytic CO_2 Reduction to Formate Using a Mn(I) Molecular Catalyst in a Robust Metal−Organic Framework. *Inorg. Chem.* **2015**, *54*, 6821−6828. (c) Wang, X.; Thiel, I.; Fedorov, A.; Copéret, C.; Mougel, V.; Fontecave, M. Site-isolated manganese carbonyl on bipyridine-functionalities of periodic mesoporous organosilicas: efficient CO_2 photoreduction and detection of key reaction intermediates. *Chem. Sci.* **2017**, *8*, 8204−8213. (d) Takeda, H.; Kamiyama, H.; Okamoto, K.; Irimajiri, M.; Mizutani, T.; Koike, K.; Sekine, A.; Ishitani, O. Highly Efficient and Robust Photocatalytic Systems for CO_2 Reduction Consisting of a Cu(I) Photosensitizer and Mn(I) Catalysts. *J. Am. Chem. Soc.* **2018**, *140*, 17241−17254. (e) Le-Quang, L.; Stanbury, M.; Chardon-Noblat, S.; Mouesca, J.-M.; Maurel, V.; Chauvin, J. Immobilization of Mn(i) and Ru(ii) polypyridyl complexes on TiO_2 nanoparticles for selective photoreduction of CO_2 to formic acid. *Chem. Commun.* **2019**, *55*, 13598−13601.

(13) Madsen, M. R.; Rønne, M. H.; Heuschen, M.; Golo, D.; Ahlquist, M. S. G.; Skrydstrup, T.; Pedersen, S. U.; Daasbjerg, K. Promoting Selective Generation of Formic Acid from CO_2 Using Mn(bpy)-$(CO)_3$Br as Electrocatalyst and Triethylamine/Isopropanol as Additives. *J. Am. Chem. Soc.* **2021**, *143*, 20491−20500.

(14) Dey, S.; Masero, F.; Brack, E.; Fontecave, M.; Mougel, V. Electrocatalytic metal hydride generation using CPET mediators. *Nature* **2022**, *607*, 499−506.

(15) Neri, G.; Walsh, J. J.; Teobaldi, G.; Donaldson, P. M.; Cowan, A. J. Detection of catalytic intermediates at an electrode surface during carbon dioxide reduction by an earth-abundant catalyst. *Nat. Catal.* **2018**, *1*, 952−959.

(16) Bhattacharya, M.; Sebghati, S.; VanderLinden, R. T.; Saouma, C. T. Toward Combined Carbon Capture and Recycling: Addition of an Amine Alters Product Selectivity from CO to Formic Acid in Manganese Catalyzed Reduction of CO_2. *J. Am. Chem. Soc.* **2020**, *142*, 17589−17597.

(17) (a) Franco, F.; Pinto, M. F.; Royo, B.; Lloret-Fillol, J. A Highly Active N-Heterocyclic Carbene Manganese(I) Complex for Selective Electrocatalytic CO_2 Reduction to CO. *Angew. Chem., Int. Ed.* **2018**, *57*, 4603−4606. (b) Myren, T. H. T.; Lilio, A. M.; Huntzinger, C. G.; Horstman, J. W.; Stinson, T. A.; Franklin, T.; Moore, C.; Lama, B.; Funke, H. H.; Luca, O. R. Manganese N-Heterocyclic Carbene Pincers for the Electrocatalytic Reduction of Carbon Dioxide. *Organometallics* **2019**, *38*, 1248−1253. (c) Myren, T. H. T.; Alherz, A.; Thurston, J. R.; Stinson, T. A.; Huntzinger, C. G.; Musgrave, C. B.; Luca, O. R. Mn-Based Molecular Catalysts for the Electrocatalytic Disproportionation of CO_2 into CO and CO_3^{-2}. *ACS Catal.* **2020**, *10*, 1961−1968. (d) Yang, Y.; Zhang, Z.; Chang, X.; Zhang, Y.-Q.; Liao, R.-Z.; Duan, L. Highly Active Manganese-Based CO_2 Reduction Catalysts with Bulky NHC Ligands: A Mechanistic Study. *Inorg. Chem.* **2020**, *59*, 10234−10242. (e) Agarwal, J.; Shaw, T. W.; Stanton Iii, C. J.; Majetich, G. F.; Bocarsly, A. B.; Schaefer Iii, H. F. NHC-Containing Manganese(I) Electrocatalysts for the Two-Electron Reduction of CO_2. *Angew. Chem., Int. Ed.* **2014**, *53*, 5152−5155.

(18) Pinto, M.; Friães, S.; Franco, F.; Lloret-Fillol, J.; Royo, B. Manganese N-Heterocyclic Carbene Complexes for Catalytic Reduction of Ketones with Silanes. *ChemCatChem* **2018**, *10*, 2734−2740.

(19) (a) Bolinger, C. M.; Story, N.; Sullivan, B. P.; Meyer, T. J. Electrocatalytic reduction of carbon dioxide by 2,2′-bipyridine complexes of rhodium and iridium. *Inorg. Chem.* **1988**, *27*, 4582−4587. (b) Slater, S.; Wagenknecht, J. H. Electrochemical reduction of carbon dioxide catalyzed by $Rh(diphos)_2Cl$. *J. Am. Chem. Soc.* **1984**, *106*, 5367−5368.

(20) Oberem, E.; Roesel, A. F.; Rosas-Hernández, A.; Kull, T.; Fischer, S.; Spannenberg, A.; Junge, H.; Beller, M.; Ludwig, R.; Roemelt, M.; Francke, R. Mechanistic Insights into the Electrochemical Reduction of CO_2 Catalyzed by Iron Cyclopentadienone Complexes. *Organometallics* **2019**, *38*, 1236−1247.

(21) Huang, M.; Li, Y.; Li, Y.; Liu, J.; Shu, S.; Liu, Y.; Ke, Z. Room temperature N-heterocyclic carbene manganese catalyzed selective N-alkylation of anilines with alcohols. *Chem. Commun.* **2019**, *55*, 6213−6216.

(22) Lan, X.-B.; Ye, Z.; Huang, M.; Liu, J.; Liu, Y.; Ke, Z. Nonbifunctional Outer-Sphere Strategy Achieved Highly Active α-Alkylation of Ketones with Alcohols by N-Heterocyclic Carbene Manganese (NHC-Mn). *Org. Lett.* **2019**, *21*, 8065−8070.

(23) Machan, C. W.; Stanton, C. J.; Vandezande, J. E.; Majetich, G. F.; Schaefer, H. F.; Kubiak, C. P.; Agarwal, J. Electrocatalytic Reduction of Carbon Dioxide by $Mn(CN)(2,2'\text{-bipyridine})(CO)_3$: CN Coordination Alters Mechanism. *Inorg. Chem.* **2015**, *54*, 8849−8856.

(24) Fernández, S.; Franco, F.; Casadevall, C.; Martin-Diaconescu, V.; Luis, J. M.; Lloret-Fillol, J. A Unified Electro- and Photocatalytic CO_2 to CO Reduction Mechanism with Aminopyridine Cobalt Complexes. *J. Am. Chem. Soc.* **2020**, *142*, 120−133.

(25) Kuo, H.-Y.; Tignor, S. E.; Lee, T. S.; Ni, D.; Park, J. E.; Scholes, G. D.; Bocarsly, A. B. Reduction-induced CO dissociation by a $[Mn(bpy)(CO)_4][SbF_6]$ complex and its relevance in electrocatalytic CO_2 reduction. *Dalton Trans.* **2020**, *49*, 891−900.

(26) Krejčik, M.; Daněk, M.; Hartl, F. Simple construction of an infrared optically transparent thin-layer electrochemical cell: Applications to the redox reactions of ferrocene, $Mn_2(CO)_{10}$ and Mn(CO)-3(3,5-di-t-butyl-catecholate)−. *J. Electroanal. Chem. Interfacial Electrochem.* **1991**, *317*, 179−187.

(27) (a) Léval, A.; Agapova, A.; Steinlechner, C.; Alberico, E.; Junge, H.; Beller, M. Hydrogen production from formic acid catalyzed by a phosphine free manganese complex: investigation and mechanistic insights. *Green Chem.* **2020**, *22*, 913−920. (b) Bertini, F.; Glatz, M.; Gorgas, N.; Stöger, B.; Peruzzini, M.; Veiros, L. F.; Kirchner, K.; Gonsalvi, L. Carbon dioxide hydrogenation catalysed by well-defined Mn(i) PNP pincer hydride complexes. *Chem. Sci.* **2017**, *8*, 5024−5029. (c) Bertini, F.; Glatz, M.; Stöger, B.; Peruzzini, M.; Veiros, L. F.; Kirchner, K.; Gonsalvi, L. Carbon Dioxide Reduction to Methanol Catalyzed by Mn(I) PNP Pincer Complexes under Mild Reaction Conditions. *ACS Catal.* **2019**, *9*, 632−639.

(28) Sampaio, R. N.; Grills, D. C.; Polyansky, D. E.; Szalda, D. J.; Fujita, E. Unexpected Roles of Triethanolamine in the Photochemical Reduction of CO_2 to Formate by Ruthenium Complexes. *J. Am. Chem. Soc.* **2020**, *142*, 2413−2428.

(29) (a) Hawecker, J.; Lehn, J.-M.; Ziessel, R. Photochemical and Electrochemical Reduction of Carbon Dioxide to Carbon Monoxide Mediated by (2,2′-Bipyridine)tricarbonylchlororhenium(I) and Related Complexes as Homogeneous Catalysts. *Helv. Chim. Acta* **1986**, *69*, 1990−2012. (b) Sampson, M. D.; Froehlich, J. D.; Smieja, J. M.; Benson, E. E.; Sharp, I. D.; Kubiak, C. P. Direct observation of the reduction of carbon dioxide by rhenium bipyridine catalysts. *Energy Environ. Sci.* **2013**, *6*, 3748−3755.

(30) Grills, D. C.; Farrington, J. A.; Layne, B. H.; Lymar, S. V.; Mello, B. A.; Preses, J. M.; Wishart, J. F. Mechanism of the Formation of a Mn-Based CO_2 Reduction Catalyst Revealed by Pulse Radiolysis with Time-Resolved Infrared Detection. *J. Am. Chem. Soc.* **2014**, *136*, 5563−5566.

(31) (a) Wiedner, E. S.; Chambers, M. B.; Pitman, C. L.; Bullock, R. M.; Miller, A. J. M.; Appel, A. M. Thermodynamic Hydricity of Transition Metal Hydrides. *Chem. Rev.* **2016**, *116*, 8655−8692. (b) Waldie, K. M.; Ostericher, A. L.; Reineke, M. H.; Sasayama, A. F.; Kubiak, C. P. Hydricity of Transition-Metal Hydrides: Thermodynamic Considerations for CO_2 Reduction. *ACS Catal.* **2018**, *8*, 1313−1324.

(32) (a) Felton, G. A. N.; Vannucci, A. K.; Okumura, N.; Lockett, L. T.; Evans, D. H.; Glass, R. S.; Lichtenberger, D. L. Hydrogen Generation from Weak Acids: Electrochemical and Computational Studies in the $[(\eta^5\text{-}C_5H_5)Fe(CO)_2]_2$ System. *Organometallics* **2008**, *27*, 4671−4679. (b) McCarthy, B. D.; Martin, D. J.; Rountree, E. S.; Ullman, A. C.; Dempsey, J. L. Electrochemical Reduction of Brønsted Acids by Glassy Carbon in Acetonitrile—Implications for Electrocatalytic Hydrogen Evolution. *Inorg. Chem.* **2014**, *53*, 8350−8361.

(33) Pugh, J. R.; Bruce, M. R. M.; Sullivan, B. P.; Meyer, T. J. Formation of a metal-hydride bond and the insertion of carbon dioxide. Key steps in the electrocatalytic reduction of carbon dioxide to formate anion. *Inorg. Chem.* **1991**, *30*, 86−91.